Headline Articles

Syntheses and Characterization of Cubane-Type Clusters with Molybdenum–Iron–Sulfur (Mo_3FeS_4) or Molybdenum–Nickel–Sulfur (Mo_3NiS_4) Cores. X-Ray Structures of $[Mo_3FeS_4(H_2O)_{10}](CH_3C_6H_4SO_3)_4\cdot 7H_2O$ and $[Mo_3FeS_4(H_2O)(NH_3)_9]Cl_4$, and Discrete Variational (DV)-Xα Calculation of the Electronic Structures of $[Mo_3FeS_4(H_2O)_{10}]^{4+}$, $[Mo_3FeS_4(H_2O)(NH_3)_9]^{4+}$, and $[Mo_3NiS_4(H_2O)_{10}]^{4+}$

Takashi Shibahara,* Genta Sakane, Yoshiyuki Naruse, Kazuhisa Taya, Haruo Akashi,† Akio Ichimura,†† and Hirohiko Adachi†††

Department of Chemistry, Okayama University of Science, 1-1 Ridai-cho, Okayama 700

†Research Institute of Natural Sciences, Okayama University of Science, 1-1 Ridai-cho, Okayama 700

††Department of Chemistry, Faculty of Science, Osaka City University, Sugimoto, Sumiyoshi-ku, Osaka 558

†††Department of Materials Science and Engineering, Kyoto University, Yoshida-honmachi, Sakyo-ku, Kyoto 606-01

(Received January 31, 1995)

Reaction of the incomplete cubane-type cluster $[Mo_3S_4(H_2O)_9]^{4+}$ (**A**) with iron gives a novel cubane-type aqua cluster $[Mo_3FeS_4(H_2O)_{10}](CH_3C_6H_4SO_3)_4\cdot 7H_2O$ (**B′**). An ammonia coordinated derivative cluster $[Mo_3FeS_4(H_2O)(NH_3)_9]Cl_4$ (**C′**) is also synthesized. X-ray structural analyses of **B′** and **C′** revealed that the clusters, $[Mo_3FeS_4(H_2O)_{10}]^{4+}$ (**B**) and $[Mo_3FeS_4(H_2O)(NH_3)_9]^{4+}$ (**C**), have an approximate symmetry of C_{3v}. The iron atom has fairly regular tetrahedral geometry in both clusters. The effective magnetic moments of **B′** at 2.16 K and 269.95 K are 2.78 and 3.26 B.M., respectively. ^{57}Fe-Mössbauer spectroscopy showed that the oxidation states of iron in **B′** and **C′** were assignable to be +2.39 and +2.54, respectively, which indicates that the reaction is a reductive addition of an iron atom to the Mo_3S_4 core in **A**. The cyclic voltammograms of **A**, **B**, and $[Mo_3NiS_4(H_2O)_{10}]^{4+}$ (**D**) show three consecutive one electron reductive steps, respectively, and the oxidation states of metals in **B** and **D** are assigned as $Mo^{IV}Mo_2^{III}M^{II}$ (M=Fe, Ni). Discrete variational (DV)-Xα calculation of **B**, **C**, and **D** explains the magnetic behavior, XPS spectra, and reactivity toward CO, C_2H_2, and C_2H_4.

We have made a preliminary report[1] on a reaction of the incomplete cubane-type sulfur-bridged molybdenum aqua cluster $[Mo_3S_4(H_2O)_9]^{4+}$ (**A**) with iron metal to give the molybdenum–iron mixed-metal cluster $[Mo_3FeS_4(H_2O)_{10}]^{4+}$ (**B**) as shown in Scheme 1. This is the first example of a reaction in which the missing corner of the incomplete cubane-type core is filled with another metal atom. Then, many metal incorporation reactions of the aqua cluster have been reported by us[2] and by other groups[3] to give mixed-metal clusters with Mo_3MS_4 cores (M=metal): not only direct reaction of **A** with metals or metal ion (Sn^{2+}), but also $NaBH_4$ reduction of **A** in the presence of M^{2+} has been used,[3b,3c] and the reaction of **A** with $[Cr(H_2O)_6]^{2+}$ to give $[Mo_3CrS_4(H_2O)_{12}]^{4+}$ has also been reported very recently.[3d] Other routes to the clusters with Mo_3MS_4

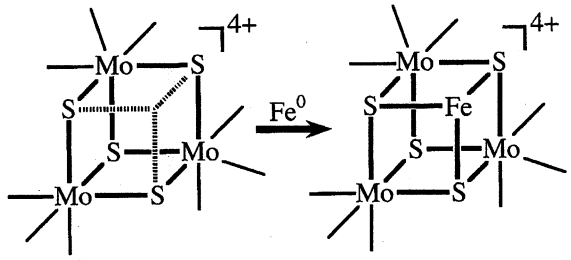

Scheme 1. Formation of mixed metal cluster $[Mo_3FeS_4(H_2O)_{10}]^{4+}$ (**B**). Coordinated H_2O's are omitted for clarity.

cores (M=Cu,[4a,4c] M=Sb,[4b,4c] M=W[5]) have also been reported.

The aqua cluster **A** reacts not only with metals as stated above but also with acetylene to give a cluster with carbon–sulfur bonds $[Mo_3(\mu_3\text{-}S)(\mu\text{-}S)(\mu_3\text{-}S_2C_2H_2)(H_2O)_9]^{4+}$.[6] On the other hand, the oxygen-bridged cluster $[Mo_3O_4(H_2O)_9]^{4+}$ (**E**) does not react either with metals[1] or acetylenes.[7]

The metal atom replacement reaction of the incorporated metal atom M in the cubane-type Mo_3MS_4 core with Cu^{2+} to give the $Mo_3CuS_4{}^{4+}$ core has been reported,[8] and the existence of a new oxidation state of $Mo_3CuS_4{}^{5+}$ is known.[9] The strong coloration on the reaction of the cluster **A** with mercury can be used for the measurement of mercury.[10] The reactivity of clusters with the Mo_3PdS_4[11] or Mo_3NiS_4[12] core toward small molecules such as CO, alkenes, and alkynes has been reported.

We report here syntheses, characterization, and X-ray structures of two cubane-type mixed-metal clusters with Mo_3FeS_4 cores, $[Mo_3FeS_4(H_2O)_{10}](CH_3C_6H_4SO_3)_4\cdot 7H_2O$ (**B′**) and $[Mo_3FeS_4(H_2O)(NH_3)_9]Cl_4$ (**C′**), and characterization of the molybdenum– nickel cluster $[Mo_3NiS_4(H_2O)_{10}](CH_3C_6H_4SO_3)_4\cdot 7H_2O$ (**D′**). Discrete Variational (DV)-Xα calculations of the clusters **B**, $[Mo_3FeS_4(H_2O)(NH_3)_9]^{4+}$ (**C**), and $[Mo_3NiS_4(H_2O)_{10}]^{4+}$ (**D**) are also described.

Experimental

Materials. *p*-Toluenesulfonic acid (Hpts) was used after recrystallization from water. Acetonitrile was purified by distillation. Ammonia water and iron (powder, wire) were used as received. The molybdenum cluster $[Mo_3S_4(H_2O)_9](CH_3C_6H_4SO_3)_4\cdot 9H_2O$ (**A′**)[13] and the molybdenum–nickel cluster **D′** [2b] were obtained by the published procedures.

Syntheses of Compounds. All the procedures were done under a dinitrogen atmosphere.

$[Mo_3FeS_4(H_2O)_{10}](CH_3C_6H_4SO_3)_4\cdot 7H_2O$ (B′):

Method A. An iron wire (3 g) was introduced into a conical flask containing the aqua ion **A** (0.05 M per trimer, 25 mL; 1 M=1 mol dm^{-3}) in 2 M HCl. During stirring, the color of the solution turned from green to red-purple in a few hours. After the remaining iron was removed, the resultant solution was absorbed on a Dowex® 50W-X2 cation exchanger (diameter 2.2 cm, length 80 cm). Iron(II) ion was eluted with 0.5 M HCl and a red-purple eluent containing **B** was obtained by the use of 1 M HCl: yield 78% based on **A**.[14] This was analyzed to give Mo/Fe=2.93±0.15 (three measurements). The green band of the unreacted starting material **A** (11%) followed the red-purple band.

In order to obtain crystals of **B′**, the solution of **B** in 1 M HCl was absorbed on a short cation exchanger, Dowex®-50W-X2 (diameter 2.2 cm, length 5 cm). The resin was washed with 0.1 M Hpts to remove chloride ion, and a red-purple solution was obtained by slow elusion with 4 M Hpts. The concentrated part of the eluate from the column was stored in a refrigerator. After one week black plate crystals deposited, which were collected by filtration, washed with ethyl acetate, and air-dried: yield 0.92 g, ca. 65% based on **B** in 1 M HCl. Anal. Found: Mo, 19.56; Fe, 3.90; C, 22.92; H, 3.66%. Calcd for $Mo_3FeS_8O_{29}C_{28}H_{62}$ (MW=1462.98): Mo, 19.67; Fe, 3.82; C, 22.99; H, 4.27%.

Method B. An iron powder (0.4 g) was introduced into a conical flask containing the aqua ion **A** (0.05 M per trimer, 25 mL; Fe/**A**=ca. 11) in 4 M Hpts. The mixture was heated at above 90 °C for 1 h with stirring in a water-bath, which was then brought to room temperature and filtered to remove the remaining iron (ca. 0.2 g) and white precipitates (mainly $Fe(pts)_2\cdot nH_2O$). Three grams of Hpts was added to the filtrate, which was kept in a refrigerator (ca. −10 °C) for 4 d. The black crystals obtained were treated as noted in Method A. Yield 0.40 g, 45% based on **A**.

$[Mo_3FeS_4(H_2O)(NH_3)_9]Cl_4$ (C′): The red-purple solution of **B** (0.05 M, 20 mL) in 1 M HCl obtained by Method A was introduced into an ice-cooled flask containing concentrated aqueous ammonia (20 mL). Black-purple crystals **C′** deposited in a few days, which was washed with a small amount of ammonia–water, and dried with methanol: yield 0.53 g, 68%. Anal. Found: NH_3, 19.49; N, 16.29; Cl, 17.76%. Calcd for $Mo_3FeCl_4S_4ON_9H_{29}$ (MW=785.03): NH_3, 19.78; N, 16.06; Cl, 18.06%.

X-Ray Structures of $[Mo_3FeS_4(H_2O)_{10}](CH_3C_6H_4SO_3)_4\cdot 7H_2O$ (B′) and $[Mo_3FeS_4(H_2O)(NH_3)_9]Cl_4$ (C′). A deep purple crystal (dimensions 0.60×0.25×0.15 mm) of **B′** and a black-purple crystal (dimensions 0.29×0.26×0.22 mm) of **C′** were mounted in glass capillaries with an adhesive. The crystallographic and machine data for **B′** and **C′** are given in Table 1. Systematic absences uniquely identified the space group as $P2_1cn$ for compound **C′**. Cell constants and orientation matrixes for the crystals **B′** and **C′** were obtained from least squares refinement, by using setting angles of 25 reflections for both the crystals in the range $20° < 2\theta < 30°$ measured on a Rigaku AFC-6S diffractometer by use of Mo $K\alpha$ radiation (λ=0.71073 Å). The intensities of the standard reflections monitored after every 150 reflections did not show any appreciable decay for the two crystals. Intensities were corrected for polarization and Lorentz factors. Absorption correction was not applied.

The compound **B′** is isomorphous with the corresponding nickel–molybdenum cluster, **D′**,[2a,2b] and the solution was straightforward: the coordinates of Mo, Ni, and S atoms of **D′** are used to solve the structure of **B′**. For compound **C′** the coordinates of Mo, Fe, and S atoms that composed the core were determined by SHELXS-86,[15] and the remaining non-hydrogen atoms were located from difference maps. No attempt was made to locate hydrogen atoms for each structure determination. The refinement of the structures

Table 1. Crystallographic Data for $[Mo_3FeS_4(H_2O)_{10}](CH_3C_6H_4SO_3)_4 \cdot 7H_2O$ (**B′**) and $[Mo_3FeS_4(H_2O)(NH_3)_9]Cl_4$ (**C′**)

	B′	**C′**
Formula	$Mo_3FeS_8O_{29}C_{28}H_{62}$	$Mo_3FeCl_4S_4ON_9H_{29}$
Fw	1462.98	785.03
Space group	$P\bar{1}$	$P2_1cn$
Syst absences		$h0l$: $l=2n+1$
		$hk0$: $h+k=2n+1$
		$h00$: $h=2n+1$
		$0k0$: $k=2n+1$
		$00l$: $l=2n+1$
a/Å	17.935(8)	14.948(4)
b/Å	19.539(8)	16.233(3)
c/Å	9.070(4)	9.208(2)
α/deg	103.15(4)	
β/deg	103.92(4)	
γ/deg	62.45(3)	
V/Å^3	2710.2(22)	2234.3(8)
Z	2	4
T/°C	18	18
λ(Mo $K\alpha$)/Å	0.71073	0.71073
d_{calcd}/g cm^{-3}	1.793	2.334
μ/cm^{-1}	13.0	31.0
$R(F_o)$/%	4.95	4.09
$R_W(F_o)$/%	6.92	5.38

was done at initial stage by the block-diagonal least squares method using the programs in the UNICS system[16] and at a later stage by the full-matrix least squares program CRYSTAN.[17] The program ORTEP[18] was used to draw perspective views. Atomic scattering factors for Mo^0, Fe^0, S^0, Cl^0, O^0, N^0, and C^0 were taken from Ref. 19. Computations were done on a FACOM M380 computer at Okayama University of Science. The atomic coordinates and thermal parameters for **B′** and **C′** are listed in Tables 2 and 3, respectively.

Computational Procedures. The computational details of the DV-Xα method used in this work have been described elsewhere.[20] The atomic radius R_0 for each atom was obtained from values determined by Slater.[21] Numerical atomic orbitals (Mo, 1s-5p; Fe, 1s-4p; S, 1s-3d; O, 1s-2p; N, 1s-2p; H, 1s) were used as basis sets for the MO calculations. The Slater exchange parameter was chosen to be α=0.7 for all atoms. The structural parameters of **B**, **C**, and **D** were idealized to C_s symmetry (The z–x plane was taken as the mirror plane). The molecular geometry of **B** is shown in Fig. 1. The atomic coordinates for **B**, **C**, and **D** were obtained from **B′**, **C′**, and **D′**. Hydrogen atoms attached to the oxygen atom trans to μ_3-S (on z-axis) were positioned on the C_s mirror plane; those attached to the oxygen atom cis to μ_3-S (on z-axis) were positioned so as to lie on the plane determined by the molybdenum atom coordinated by the water molecule, the oxygen atom, and the gravity center of the three molybdenum atoms.

The sample points were taken up to 50000 points for each calculation. Self-consistency within 0.003 e was obtained for the orbital populations. The calculations were done on a Hewlett–Packard HP-Apollo 9000/730 computer at Okayama University of Science.

Electrochemical Measurement. Cyclic voltammetry of the clusters **A′**, **B′**, and **D′** was done with a Fuso potentiostat HECS-972W in acetonitrile with 0.1 M tetrabuthylammonium hexafluorophosphate was used as solvent. The working electrode was a glassy carbon. The reference and the counter electrodes were Ag/Ag^+ and a platinum wire, respectively. A redox potential of ferricinium/ferrocene couple was +0.094 V with respect to this reference electrode.

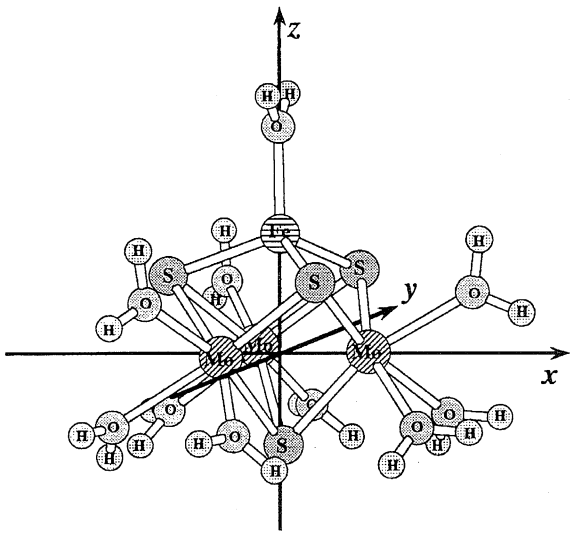

Fig. 1. Molecular geometry of $[Mo_3FeS_4(H_2O)_{10}]^{4+}$ (**B**).

Apparatus. The XPS measurements were done with a Shimadzu ESCA 850 using Mg $K\alpha$ radiation at Research Instruments Center, Okayama University of Science. UV, visible, and near-infrared spectra were recorded on a Hitachi 330, 320, or U2000 spectrophotometer. ICP spectrometry was used for the analysis of molybdenum and iron using a Shimadzu ICPS-500 analyzer. Carbon, hydrogen, and nitrogen were determined with a Perkin–Elmer 240 NCH analyzer, or Yanaco CHN corder MT-3.

Results and Discussion

Syntheses and Properties of Cluster Compounds with Mo_3FeS_4 Cores. As a first example of metal incorporation reaction, a very interesting feature was yielded when the molybdenum aqua cluster **A** reacted with an elemental iron to give the molybdenum–iron mixed-metal cluster **B**. Many metal incorporation reactions of the aqua cluster have since been reported, as stated above. This is in remarkable contrast to the case of the reaction of the oxygen-bridged cluster **E** with iron, reaction product being simply the reduced form of **E** with no incorporation of an iron atom.[1] We can think of two kinds of driving forces for the formation of the cubane-type mixed-metal clusters from the incomplete cubane-type aqua cluster **A** and metals. One factor is the affinity of the metal for the bridging sulfur atoms, and another is the reducing ability of the metal.[1,2b] Both factors seem responsible for the formation of **B**.

Two methods are described here for the synthesis of the aqua cluster **B**. Method A uses 2 M HCl as a solvent for the reaction of **A** with iron.[1] The reaction products

Table 2. Atomic Coordinates and Equivalent Isotropic Temperature Factors for $[Mo_3FeS_4(H_2O)_{10}](CH_3C_6H_4SO_3)_4 \cdot 7H_2O$ (**B′**)

Atom	x	y	z	B_{eq}[a]/Å^2	Atom	x	y	z	B_{eq}[a]/Å^2
Mo1	1.06705(3)	0.67627(2)	0.55279(5)	2.01(2)	CP13	1.4724(5)	0.3286(5)	1.1242(8)	5.8(3)
Mo2	0.94526(3)	0.82877(2)	0.58143(5)	1.99(2)	CP14	1.5121(5)	0.3761(6)	1.1391(8)	6.2(3)
Mo3	1.05248(3)	0.76504(2)	0.83932(5)	1.88(2)	CP15	1.4607(4)	0.4545(5)	1.1197(8)	5.4(3)
Fe	1.11156(4)	0.79430(4)	0.6300(1)	2.35(3)	CP16	1.3704(4)	0.4854(4)	1.0811(7)	4.3(3)
S1	0.9504(1)	0.7259(1)	0.6830(1)	2.28(4)	CP17	1.6088(5)	0.3464(7)	1.177(1)	10.0(5)
S2	1.0400(1)	0.7705(1)	0.4002(1)	2.52(4)	CP21	1.4099(3)	0.6515(3)	0.3493(6)	2.9(2)
S3	1.0180(1)	0.8877(1)	0.7773(1)	2.40(4)	CP22	1.4455(4)	0.6700(4)	0.2512(7)	4.1(3)
S4	1.1795(1)	0.6850(1)	0.7400(1)	2.42(4)	CP23	1.5336(4)	0.6401(4)	0.2671(8)	4.6(3)
SP1	1.2244(1)	0.4682(1)	1.0041(2)	3.6(1)	CP24	1.5865(4)	0.5936(4)	0.3779(8)	4.3(2)
SP2	1.2974(1)	0.6943(1)	0.3359(2)	3.4(1)	CP25	1.5496(4)	0.5755(4)	0.4732(9)	5.1(3)
SP3	1.2400(1)	0.9237(1)	1.0004(2)	4.1(1)	CP26	1.4611(4)	0.6039(4)	0.4586(7)	4.2(3)
SP4	0.7064(1)	0.7963(1)	0.6626(2)	5.0(1)	CP27	1.6841(4)	0.5619(5)	0.396(1)	6.4(3)
O11	1.1691(2)	0.5987(2)	0.4131(4)	3.4(1)	CP31	1.3485(4)	0.9051(3)	1.0473(7)	3.4(2)
O12	0.9957(2)	0.6263(2)	0.3662(4)	3.6(1)	CP32	1.3840(5)	0.9280(5)	0.9612(9)	6.0(4)
O13	1.1006(2)	0.5627(2)	0.6236(5)	3.6(1)	CP33	1.4731(5)	0.9073(6)	0.996(1)	6.6(4)
O21	0.8955(2)	0.9340(2)	0.4683(4)	3.1(1)	CP34	1.5211(5)	0.8679(5)	1.1163(9)	5.8(3)
O22	0.8301(2)	0.9008(2)	0.6879(4)	3.6(1)	CP35	1.4833(5)	0.8459(5)	1.205(1)	6.1(3)
O23	0.8472(2)	0.8097(2)	0.3986(4)	3.6(1)	CP36	1.3979(5)	0.8636(4)	1.1697(8)	5.3(3)
O31	1.1321(2)	0.7979(2)	1.0422(4)	2.9(1)	CP37	1.6176(5)	0.8445(6)	1.148(1)	8.4(5)
O32	1.0880(2)	0.6758(2)	0.9834(4)	3.2(1)	CP41	0.5934(4)	0.8408(4)	0.6419(7)	3.9(2)
O33	0.9610(2)	0.8253(2)	1.0041(4)	3.3(1)	CP42	0.5499(4)	0.9209(4)	0.6438(9)	4.8(3)
O	1.1880(3)	0.8392(2)	0.6188(4)	3.8(2)	CP43	0.4610(5)	0.9541(4)	0.6106(9)	5.3(3)
OP11	1.1831(3)	0.4971(3)	1.1418(5)	5.0(2)	CP44	0.4160(4)	0.9091(4)	0.5843(8)	4.8(3)
OP12	1.2004(3)	0.5299(2)	0.9108(5)	4.7(2)	CP45	0.4641(4)	0.8285(4)	0.5814(8)	4.5(3)
OP13	1.2089(3)	0.4032(3)	0.9150(5)	5.1(2)	CP46	0.5513(4)	0.7935(4)	0.6095(8)	4.5(3)
OP21	1.2715(3)	0.7772(2)	0.3894(5)	4.3(2)	CP47	0.3178(5)	0.9484(6)	0.547(1)	7.6(4)
OP22	1.2635(3)	0.6807(3)	0.1749(4)	4.4(2)	OW1	0.8712(3)	1.0682(2)	0.6713(5)	4.0(2)
OP23	1.2785(3)	0.6582(3)	0.4349(6)	5.1(2)	OW2	0.9666(3)	0.9377(2)	0.2383(4)	3.8(2)
OP31	1.1981(4)	0.9656(3)	1.1318(7)	7.0(3)	OW3	0.8427(4)	0.6411(4)	0.3848(6)	8.4(3)
OP32	1.2386(3)	0.8480(3)	0.9654(8)	7.9(3)	OW4	0.9715(5)	0.6526(5)	0.0727(6)	10.0(5)
OP33	1.2066(3)	0.9588(5)	0.8645(8)	10.0(4)	OW5	0.8100(5)	0.8600(5)	0.1133(8)	10.8(5)
OP41	0.7372(4)	0.8418(4)	0.7783(8)	9.0(3)	OW6A	0.8107(7)	0.7101(6)	0.991(1)	8.2(3)[b]
OP42	0.7370(3)	0.7170(3)	0.6816(9)	9.3(3)	OW6B	0.865(1)	0.6243(9)	0.853(2)	7.2(3)[b]
OP43	0.7300(4)	0.7923(5)	0.5116(9)	10.7(4)	OW7A	0.8682(8)	0.5530(7)	0.640(1)	9.2(3)[b]
CP11	1.3360(4)	0.4329(3)	1.0587(7)	3.3(2)	OW7B	0.959(1)	0.5361(9)	0.634(2)	7.8(4)[b]
CP12	1.3837(5)	0.3553(4)	1.0847(8)	5.0(3)					

a) Equivalent isotropic temperature factors ($B_{eq}=4/3\{\Sigma\Sigma B_{ij}a_i a_j\}$). b) Isotropic temperature factors were used. The following occupancy factors were used for the disorderd atoms: OW6A, 0.6; OW6B, 0.4; OW7A, 0.6; OW7B, 0.4.

require Dowex 50W-X2 separation, 1 M HCl being an eluent. To obtain a solid sample of **B′**, Method A requires another procedure with Dowex 50W-X2 column chromatography, 4 M Hpts being used as eluent. Yields of **B** and **B′** are high: 78 and 50%, respectively, based on **A**. Method B uses 4 M Hpts as solvent from the beginning, which gives **B** (yield, ca. 100%) and then **B′** (yield, 45%). The solution of **A** in 4 M Hpts should be free from chloride ion: Chloride iron prevents the reaction product **B** from crystallizing out to give the solid sample **B′**. Since the formation of white precipitates $Fe(pts)_2 \cdot nH_2O$ reduces the concentration of pts^- anion in solution, solid Hpts should be added to the solution to increase the amount of the crystals **B′** to be formed. We have used 4 M Hpts for the synthesis of $[Mo_3InS_4(pts)_2(H_2O)_{10}](pts)_3 \cdot 13H_2O$,[2f] and now applied the method for the synthesis of the molybdenum–iron aqua cluster **B′**. The advantage of the Method B is that no column-chromatography separation is required. The disadvantage of the Method B is that the sample **B′** obtained by this method is contaminated by a few percents of white iron salt of $Fe(pts)_2 \cdot nH_2O$.

The mixed-metal cluster **B** in solution is air-sensitive, and exposure of **B** to the air gives the source cluster **A** together with iron(II) ion as shown in Eq. 1 (the cluster **B** (ca. 1 mM) in diluted HCl turns to **A** in several hours). Solid samples of **B′** and **C′** are rather stable and can be handled in the air.

$$[Mo_3FeS_4(H_2O)_{10}]^{4+} + (1/2)O_2 + 2H^+ \longrightarrow [Mo_3S_4(H_2O)_9]^{4+} + Fe^{2+}(aq) + 2H_2O \quad (1)$$

Table 3. Atomic Coordinates and Equivalent Isotropic Temperature Factors for $[Mo_3FeS_4(H_2O)(NH_3)_9]Cl_4$ (**C′**)

Atom	x	y	z	B_{eq}[a)]/Å^2
Mo1	0.0	0.0822(1)	0.1981(2)	1.09(3)
Mo2	−0.0926(2)	−0.06719(3)	0.18268(5)	1.28(1)
Mo3	−0.18612(4)	0.0817(1)	0.2007(2)	1.20(3)
Fe	−0.0919(3)	0.03948(5)	−0.0387(1)	1.55(2)
S1	−0.0942(5)	0.0251(1)	0.3808(1)	1.75(3)
S2	0.0300(4)	−0.0261(3)	0.0340(5)	1.8(1)
S3	−0.2159(3)	−0.0273(3)	0.0401(5)	1.7(1)
S4	−0.0930(4)	0.1670(1)	0.0563(1)	1.67(3)
N11	0.115(1)	0.1521(9)	0.089(2)	3.1(3)
N12	0.110(1)	0.0382(8)	0.343(2)	1.9(2)
N13	0.021(1)	0.185(1)	0.362(2)	2.6(3)
N21	−0.098(1)	−0.1813(3)	0.0394(7)	2.2(2)
N22	−0.186(1)	−0.145(1)	0.308(2)	2.9(3)
N23	0.001(1)	−0.146(1)	0.318(2)	2.2(3)
N31	−0.2952(8)	0.1480(6)	0.076(1)	1.2(2)
N32	−0.205(1)	0.192(1)	0.343(2)	2.4(3)
N33	−0.306(1)	0.037(1)	0.334(2)	2.8(3)
O	−0.098(2)	0.0304(5)	−0.2585(6)	4.9(2)
Cl1	0.0890(3)	0.1404(3)	0.6903(4)	2.4(1)
Cl2	0.2254(5)	0.6425(5)	0.8138(8)	5.6(2)
Cl3	0.2907(6)	0.1605(5)	0.3170(8)	10.1(3)
Cl4	0.5339(3)	0.1656(3)	0.3240(6)	5.5(1)

a) Equivalent isotropic temperature factors ($B_{eq}=4/3\{\Sigma\Sigma B_{ij}a_i a_j\}$).

The ammonia-coordinated cluster **C′** is easily obtained in rather good yield from **B** in 1 M HCl by the addition of concentrated ammonia water to the solution.

Electronic spectra of **B** and **C** are shown in Fig. 2 together with that of **A**. The electronic spectrum of the cluster **B** in 2 M Hpts has peaks at 995 nm (ε 141 ($M^{-1}cm^{-1}$)/mol), 600 (ε 507), 505 (ε 846), and 470 sh (ε 765): the peaks of **B** in 1 M HCl are at 960 (177), 600sh (535), 512 (830), 464 (875). The peaks of **C** in concentrated ammonia water are at 920 nm (ε 135), 602sh (ε 495), 513 (ε 756), 466 (ε, 714), 320sh (2470) (see the Figure caption).

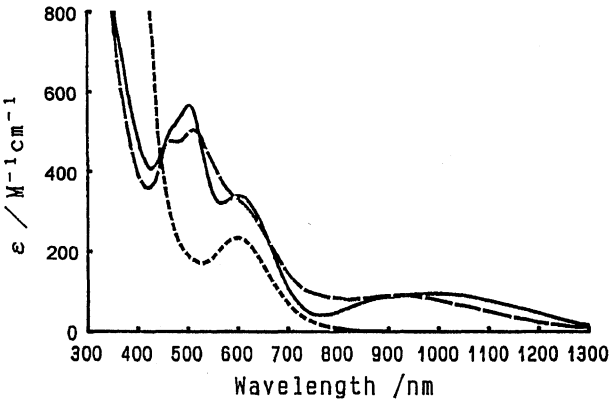

Fig. 2. Electronic spectra. —, $[Mo_3FeS_4(H_2O)_{10}]^{4+}$ (**B**) in 2 M Hpts; – – –, $[Mo_3FeS_4(H_2O)(NH_3)_9]^{4+}$ (**C**) in concentrated aqueous ammonia (In order to avoid the strong light absorption of ammonia, dilute aqueous ammonia solution (1 M) was used in 800—1300 nm region, although the spectrum is gradually changeable); - - -, $[Mo_3S_4(H_2O)_9]^{4+}$ (**A**) in 2 M Hpts.

The ^{57}Fe-Mössbauer spectroscopy showed that the oxidation states of the iron atoms in the mixed metal clusters **B′** and **C′** were assignable to be +2.39 and +2.54, respectively,[22] which indicates that the reaction is reductive addition of iron to the Mo_3S_4 core in the molybdenum aqua cluster **A**.

Although the Mo–Ni–S cluster **D** reacts with small molecules (L) such as CO, C_2H_4, and C_2H_2 to give $[Mo_3NiS_4(L)(H_2O)_9]^{4+}$,[12] the Mo–Fe–S cluster **B** does not react with these molecules. This will be discussed in the section of DV-Xα calculation.

Electrochemistry. Figure 3 shows cyclic voltammograms of **A**, **B**, and **D**. The cyclic voltammogram of **A** shows three consecutive one-electron reduction processes (the cathodic peak potentials, E_{pc}, are −0.45, −1.01, and −1.74 V, respectively), as was observed in $[M_3S_4(Hnta)_3]^{2-}$ (M_3 = Mo_3, Mo_2W, MoW_2, W_3)[23] and $[Mo_3S_4(ida)_3]^{2-}$.[24] These processes correspond to the change of oxidation states of the three metal atoms in each cluster: $Mo^{IV}{}_3 \rightarrow Mo^{IV}{}_2Mo^{III} \rightarrow Mo^{IV}Mo^{III}{}_2 \rightarrow Mo^{III}{}_3$.

The cyclic voltammogram of **B** also shows three reduction peaks with E_{pc} = −0.91, −1.47, and −1.81 V, the chemical reversibility being less. The cathodic peak currents are close to each other and almost the same as those of **A** after being normalized by concentration,

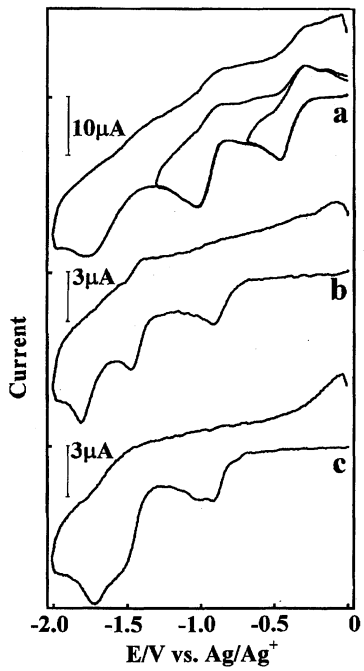

Fig. 3. Cyclic voltammograms of a) $[Mo_3S_4(H_2O)_9]^{4+}$ (**A**, 1 mM), b) $[Mo_3FeS_4(H_2O)_{10}]^{4+}$ (**B**, 0.3 mM), and c) $[Mo_3NiS_4(H_2O)_{10}]^{4+}$ (**D**, 0.3 mM) at a glassy carbon electrode in 0.1 M tetrabuthylammonium hexafluorophosphate/acetonitrile with a scan rate of 100 mV s^{-1} (see Experimental).

indicating that **B** undergoes to consecutive one-electron reduction processes. Four varieties of the oxidation states of the metals in **B** before reduction are possible: $Mo^{IV}{}_3Fe^0$, $Mo^{IV}{}_2Mo^{III}Fe^I$, $Mo^{IV}Mo^{III}{}_2Fe^{II}$, $Mo^{III}{}_3Fe^{III}$. Of these oxidation states $Mo^{IV}Mo^{III}{}_2Fe^{II}$ is most appropriate, because the oxidation state of iron atom in **B** has been determined to be +2.39 by the ^{57}Fe-Mössbauer spectroscopy.[22] After the complete reduction of **B** involving three electrons the oxidation state of the metals is $Mo^{III}{}_3Fe^0$. Three ways of reduction routes from $Mo^{IV}Mo^{III}{}_2Fe^{II}$ to $Mo^{III}{}_3Fe^0$ are possible as noted in the following Eqs. 2, 3, and 4:

$$Mo^{IV}Mo^{III}{}_2Fe^{II} \xrightarrow{e} Mo^{III}{}_3Fe^{II} \xrightarrow{e} Mo^{III}{}_3Fe^{I} \xrightarrow{e} Mo^{III}{}_3Fe^0 \quad (2)$$

$$Mo^{IV}Mo^{III}{}_2Fe^{II} \xrightarrow{e} Mo^{IV}Mo^{III}{}_2Fe^{I} \xrightarrow{e} Mo^{III}{}_3Fe^{I} \xrightarrow{e} Mo^{III}{}_3Fe^0 \quad (3)$$

$$Mo^{IV}Mo^{III}{}_2Fe^{II} \xrightarrow{e} Mo^{IV}Mo^{III}{}_2Fe^{I} \xrightarrow{e} Mo^{IV}Mo^{III}{}_2Fe^{0} \xrightarrow{e} Mo^{III}{}_3Fe^0 \quad (4)$$

We tentatively take the Eq. 4 as the reduction course, since the peak potential of the third reduction of **B** (Fig. 3b) is close to that of the third reduction of **A** (Fig. 3a) where Mo^{IV} is reduced to Mo^{III}.

The cyclic voltammogram of **D** also shows three consecutive one-electron reduction peaks with chemical irreversibility at E_{pc}=−0.91, −1.48, −1.72 V; the second peak being unclear due to the overlap of second and third peaks. The corresponding cathodic peak potentials of **B** and **D** are very close to each other. The standard potentials of $Fe^{2+/0}$ (−0.44 V) and $Ni^{2+/0}$ (−0.257 V) are also close to each other, and nickel metal is supposed to reduce the cluster **A** nearly to the same extent as iron metal reduces the cluster **A**. Therefore the oxidation states of metals in **D** is expressed as $Mo^{IV}Mo^{III}{}_2Ni^{II}$. Similarly to the reduced state of the cluster **B**, the oxidation state of the metals in **D** after three-electron reduction is expressed as $Mo^{III}{}_3Ni^0$ and the reduction course appears to be similar to the Eq. 4.

X-Ray Structures of $[Mo_3FeS_4(H_2O)_{10}](CH_3C_6H_4SO_3)_4\cdot 7H_2O$ (B′) and $[Mo_3FeS_4(H_2O)(NH_3)_9]Cl_4$ (C′). The structure of aqua cation **B** is shown in Fig. 4, and the selected interatomic distances and angles are collected in Table 4. The compound **B′** is isomorphous with the Mo–Ni–S cluster **D′**.[2a,2b] The structure of the cation of the ammonia derivative **C′** is shown in Fig. 5 and selected interatomic distances and angles are collected in Table 5. Both cluster cations have an approximate symmetry of C_{3v} (if hydrogen atoms of the water molecule coordinated to the iron atom in the respective cluster cations are ignored), and contain the cubane-type core as Mo_3FeS_4.

The introduction of an iron atom into the Mo_3S_4 core in **A′** [25] causes the following dimensional changes: the Mo–Mo distances in **B′** (2.767[7] Å) and **C′** (2.792[9] Å) are slightly longer than that in **A′** (2.735[8] Å), and the μ_3'-S–Mo–μ_3'-S angles[26] in **B′** (102.0[6]°) and **C′** (101.4[4]°) are slightly larger than the corresponding angles in **A′** (95.5[10]°). The Mo–Fe distances in **B′** (2.671[11] Å) and **C′** (2.682[19] Å) are shorter than the Mo–Mo distances in **B′** (2.767[7] Å) and **C′** (2.792[9] Å). The iron atom has a fairly regular tetrahedral geometry in **B′** and **C′**, where the iron atom is surrounded by three sulfur atoms and one oxygen atom: the S–Fe–S and S–Fe–O angles in **B′** and **C′** are close to 109°, respectively. These values in **B′** and **C′** are close to the corresponding values found in the molybdenum-nickel cluster **D′**: Mo–Mo, 2.755[10] Å; μ_3'-S–Mo–μ_3'-S,[26] 101.2[7]°; Mo–Ni, 2.640[9] Å; Mo–Mo, 2.755[10] Å; S–Ni–S, 109.6[3]°; S–Ni–O, 109.4[43]°.[2b]

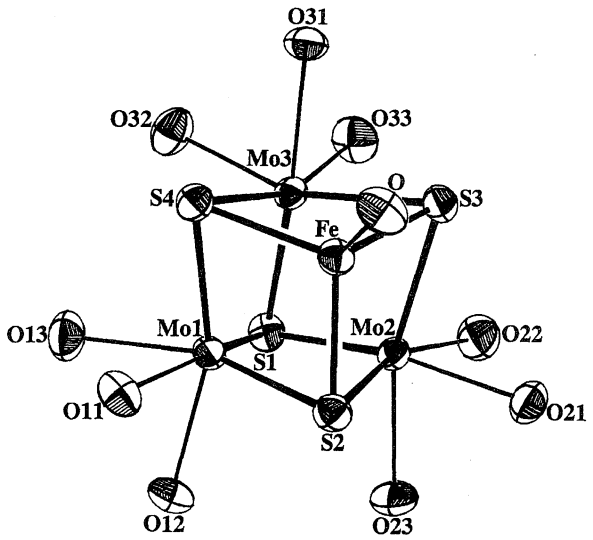

Fig. 4. Perspective view of $[Mo_3FeS_4(H_2O)_{10}]^{4+}$ (the cation of **B′**) showing the atom labeling scheme. The metal–metal bonds are not drawn for clarity, and the 50% probability vibrational ellipsoids are shown.

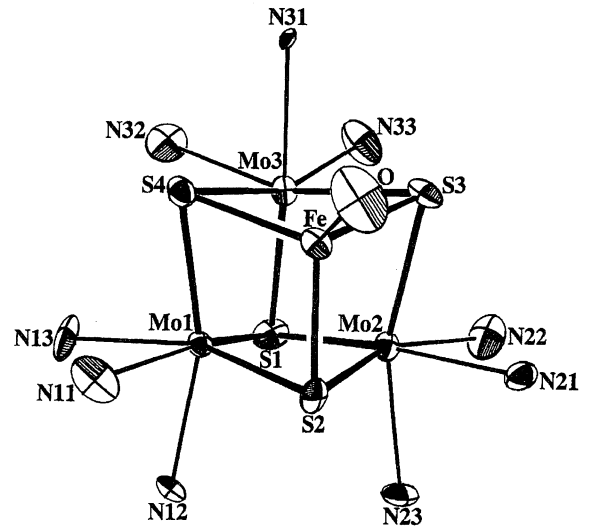

Fig. 5. Perspective view of $[Mo_3FeS_4(H_2O)(NH_3)_9]^{4+}$ (the cation of **C′**). The metal–metal bonds are not drawn for clarity, and the 50% probability vibrational ellipsoids are shown.

Magnetic Susceptibility. Magnetic susceptibil-

Table 4. Selected Interatomic Distances (Å) and Angles (deg) in $[Mo_3FeS_4(H_2O)_{10}](CH_3C_6H_4SO_3)_4 \cdot 7H_2O$ (**B′**)

Mo1–Mo2	2.760(2)	Fe–O	1.971(6)	S2–Fe–O	112.8(1)
Mo1–Mo3	2.773(2)			S3–Fe–O	103.9(1)
Mo2–Mo3	2.769(2)	Mo2–Mo1–Mo3	60.06(5)	S4–Fe–O	112.8(1)
Mean	2.767[7]	Mo1–Mo2–Mo3	60.20(5)	Mean	109.8[51]
		Mo1–Mo3–Mo2	59.75(4)		
Mo1–Fe	2.673(1)	Mean	60.00[23]	O11–Mo1–O12	80.0(2)
Mo2–Fe	2.681(2)			O11–Mo1–O13	80.3(2)
Mo3–Fe	2.660(1)	Mo2–Mo1–Fe	59.11(4)	O21–Mo2–O22	80.8(2)
Mean	2.671[11]	Mo3–Mo1–Fe	58.44(4)	O21–Mo2–O23	79.6(2)
		Mo1–Mo2–Fe	58.83(4)	O31–Mo3–O32	77.6(2)
Mo1–S1	2.346(2)	Mo3–Mo2–Fe	58.40(4)	O31–Mo3–O33	78.8(1)
Mo2–S1	2.351(2)	Mo1–Mo3–Fe	58.91(4)	Mean	79.5[12]
Mo3–S1	2.345(2)	Mo2–Mo3–Fe	58.15(4)		
Mean	2.347[3]	Mean	58.81[32]	O12–Mo1–O13	77.2(2)
				O22–Mo2–O23	79.1(1)
Mo1–S2	2.356(2)	Mo1–Fe–Mo2	62.06(4)	O32–Mo3–O33	77.4(1)
Mo1–S4	2.349(2)	Mo1–Fe–Mo3	62.65(4)	Mean	77.9[10]
Mo2–S2	2.364(2)	Mo2–Fe–Mo3	62.45(5)		
Mo2–S3	2.352(2)	Mean	62.39[30]	Mo1–S1–Mo2	72.0(1)
Mo3–S3	2.350(2)			Mo1–S1–M03	72.5(1)
Mo3–S4	2.344(2)	S1–Mo1–S2	106.6(1)	Mo2–S1–Mo3	72.3(1)
Mean	2.353[7]	S1–Mo1–S4	105.2(1)	Mean	72.3[3]
		S1–Mo2–S2	106.2(1)		
Fe–S2	2.244(2)	S1–Mo2–S3	105.5(1)	Mo1–S2–Mo2	71.6(1)
Fe–S3	2.251(2)	S1–Mo3–S3	105.8(1)	Mo2–S3–Mo3	72.2(1)
Fe–S4	2.240(2)	S1–Mo3–S4	105.4(1)	Mo1–S4–Mo3	72.4(1)
Mean	2.245[6]	Mean	105.8[5]	Mean	72.1[4]
Mo1–O11	2.220(4)	S2–Mo1–S4	101.7(1)		
Mo1–O12	2.194(4)	S2–Mo2–S3	101.6(1)	Mo1–S2–Fe	71.0(1)
Mo1–O13	2.219(5)	S3–Mo3–S4	102.7(1)	Mo2–S2–Fe	71.1(1)
Mo2–O21	2.213(4)	Mean	102.0[6]	Mo2–S3–Fe	71.2(1)
Mo2–O22	2.198(4)			Mo3–S3–Fe	70.6(1)
Mo2–O23	2.215(4)	S2–Fe–S3	108.8(1)	Mo1–S4–Fe	71.2(1)
Mo3–O31	2.210(4)	S2–Fe–S4	108.9(1)	Mo3–S4–Fe	70.9(1)
Mo3–O32	2.183(5)	S3–Fe–S4	109.4(1)	Mean	71.0[2]
Mo3–O33	2.215(4)	Mean	109.0[3]		
Mean	2.207[13]				

ities of **B′** and **D′** have been measured at temperatures from ca. 2 K through 270 K and are analyzed on the basis of the vector model formalism.[27] Both the clusters **B′** and **D′** show antiferromagnetic behavior, and the effective magnetic moments are as follows: 2.78 B.M. at 2.16 K and 3.26 B.M. at 269.95 K for **B′**; 0.11 B.M. at 2.00 K and 1.26 B.M. at 260.70 K for **D′**. Using the models of $Mo^{IV}Mo^{III}{}_2Fe^{II}$ and $Mo^{IV}Mo^{III}{}_2Ni^{II}$, we obtained the following exchange integrals: $J_{1(Mo-Mo)}/k = -25$ K, $J_{2(Mo-Fe)}/k = -75$ K for **B′**; $J_{1(Mo-Mo)}/k = -35$ K, $J_{2(Mo-Ni)}/k = -60$ K for **D′**. The incomplete cubane-type trinuclear cluster of molybdenum(IV) $Ca_{1.5}[Mo_3S_4(Hnta)(nta)_2] \cdot 12H_2O$ is diamagnetic;[28] therefore, the introduction of an iron atom into the incomplete cubane-type Mo_3S_4 core induced paramagnetism.

DV-Xα Calculation of the Electronic Structures of $[Mo_3FeS_4(H_2O)_{10}]^{4+}$ (B), $[Mo_3FeS_4(H_2O)(NH_3)_9]^{4+}$ (C), and $[Mo_3NiS_4(H_2O)_{10}]^{4+}$ (D). Charge Distribution and Energy Levels. The orbital populations and net charges obtained by Mulliken population analyses of the two clusters **B** and **D** are collected in Tables 6 and 7, respectively. The net charges of each atom are close to zero, which is consistent with Pauling's electroneutrality principle.

Energy levels for **B** (as shown in Fig. 6) show that spin polarization[29] occurs indicating paramagnetism by two electron, and those for **D** (as shown in Fig. 7) shows no spin polarization, which are consistent with the experimental results as noted in the section of Magnetic

Table 5. Selected Interatomic Distances (Å) and Angles (deg) in $[Mo_3FeS_4(H_2O)(NH_3)_9]Cl_4$ (**C'**)

Mo1–Mo2	2.797(2)	Fe–O	2.032(6)	S2–Fe–O	107.6(6)
Mo1–Mo3	2.782(1)			S3–Fe–O	104.4(6)
Mo2–Mo3	2.797(2)	Mo2–Mo1–Mo3	60.2(1)	S4–Fe–O	117.0(2)
Mean	2.792[9]	Mo1–Mo2–Mo3	59.66(3)	Mean	109.7[65]
		Mo1–Mo3–Mo2	60.2(1)		
Mo1–Fe	2.669(3)	Mean	60.0[3]	N11–Mo1–N12	82.3(5)
Mo2–Fe	2.674(1)			N11–Mo1–N13	79.7(6)
Mo3–Fe	2.704(3)	Mo2–Mo1–Fe	58.54(5)	N21–Mo2–N22	79.2(6)
Mean	2.682[19]	Mo3–Mo1–Fe	59.4(1)	N21–Mo2–N23	83.3(6)
		Mo1–Mo2–Fe	58.3(1)	N31–Mo3–N32	79.9(5)
Mo1–S1	2.381(5)	Mo3–Mo2–Fe	59.2(1)	N31–Mo3–N33	81.9(5)
Mo2–S1	2.361(2)	Mo1–Mo3–Fe	58.2(1)	Mean	81.1[17]
Mo3–S1	2.341(5)	Mo2–Mo3–Fe	58.15(5)		
Mean	2.361[20]	Mean	58.6[5]	N12–Mo1–N13	74.7(6)
				N22–Mo2–N23	77.3(6)
Mo1–S2	2.362(5)	Mo1–Fe–Mo2	63.1(1)	N32–Mo3–N33	80.8(6)
Mo1–S4	2.352(4)	Mo1–Fe–Mo3	62.37(4)	Mean	77.6[31]
Mo2–S2	2.383(5)	Mo2–Fe–Mo3	62.7(1)		
Mo2–S3	2.353(5)	Mean	62.7[4]	Mo1–S1–Mo2	72.3(1)
Mo3–S3	2.348(5)			Mo1–S1–Mo3	72.2(1)
Mo3–S4	2.372(4)	S1–Mo1–S2	105.9(1)	Mo2–S1–Mo3	73.0(1)
Mean	2.362[14]	S1–Mo1–S4	105.7(2)	Mean	72.5[4]
		S1–Mo2–S2	105.9(2)		
Fe–S2	2.213(6)	S1–Mo2–S3	104.4(2)	Mo1–S2–Mo2	72.2(1)
Fe–S3	2.266(6)	S1–Mo3–S3	105.2(1)	Mo2–S3–Mo3	73.0(1)
Fe–S4	2.247(2)	S1–Mo3–S4	106.3(2)	Mo1–S4–Mo3	72.2(1)
Mean	2.242[27]	Mean	105.6[7]	Mean	72.5[5]
Mo1–N11	2.294(15)	S2–Mo1–S4	101.1(1)	Mo1–S2–Fe	71.3(1)
Mo1–N12	2.238(15)	S2–Mo2–S3	101.8(2)	Mo2–S2–Fe	71.1(2)
Mo1–N13	2.270(17)	S3–Mo3–S4	101.4(1)	Mo2–S3–Fe	70.7(2)
Mo2–N21	2.276(6)	Mean	101.4[4]	Mo3–S3–Fe	71.7(2)
Mo2–N22	2.206(17)			Mo1–S4–Fe	70.9(1)
Mo2–N23	2.262(17)	S2–Fe–S3	110.3(2)	Mo3–S4–Fe	71.6(1)
Mo3–N31	2.268(12)	S2–Fe–S4	109.4(2)	Mean	71.2[4]
Mo3–N32	2.233(18)	S3–Fe–S4	108.1(2)		
Mo3–N33	2.295(17)	Mean	109.3[11]		
Mean	2.260[29]				

Susceptibility. In calculation addition of two electrons to **B** results in the state of no polarization.

Contour maps of HOMO for **B** and **D** are shown in Figs. 8 and 9, respectively, and atomic orbital components constituting HOMO's (a, **B** (93a' ↓); b, **D** (94a')) are shown in Fig. 10 (those of sulfurs are not shown). The molybdenum–iron and molybdenum–nickel bonds in HOMO are of bonding character and nonbonding character, respectively. The bond orders of metal–metal and metal–sulfur, and metal–oxygen bonds in **B** and **D** are shown in Fig. 11. The magnitudes of the corresponding bond orders in **B** and **D** are not so different from each other. The existence of metal–metal bonds is certain, though the magnitudes of the metal–metal bond orders are about one fourth of those of metal–sulfur bond orders.

Although the structures of **B** and **D** are very similar to each other (**B'** is isomorphous with **D'**), the reactivities toward small molecules such as carbon monoxide, ethylene and acetylene are very different from each other: **B** does not react and **D** does.[12,30] This difference may be explained by using Figs. 10 and 12. Figure 12 shows LUMO's of the small molecules.[31] In Fig. 10 the orbital component of iron (3 d_{z^2}, 27%) is smaller than that of nickel (d_{xz}, 46%), and moreover the iron orbital, which does not match the LUMO of the small molecules, can not back-donate electrons to the small molecules. Figure 13 shows effective spin density ($\Delta\rho=\rho_\uparrow-\rho_\downarrow$) of the paramagnetic species **B**, which indicates that spin density is largely located at the iron atom.

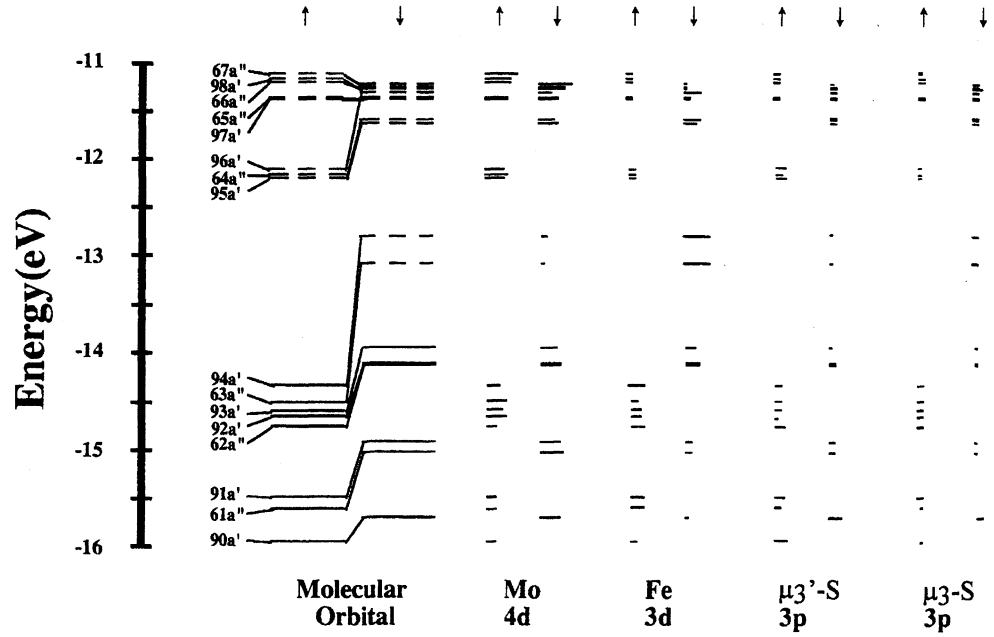

Fig. 6. Energy levels for $[Mo_3FeS_4(H_2O)_{10}]^{4+}$ (**B**). μ_3-S, sulfur atom bridging three molybdenum atoms; μ_3'-S, sulfur atom bridging two molybdenum and one iron atoms. The symbols ↑ and ↓ indicate the direction of spins, respectively.

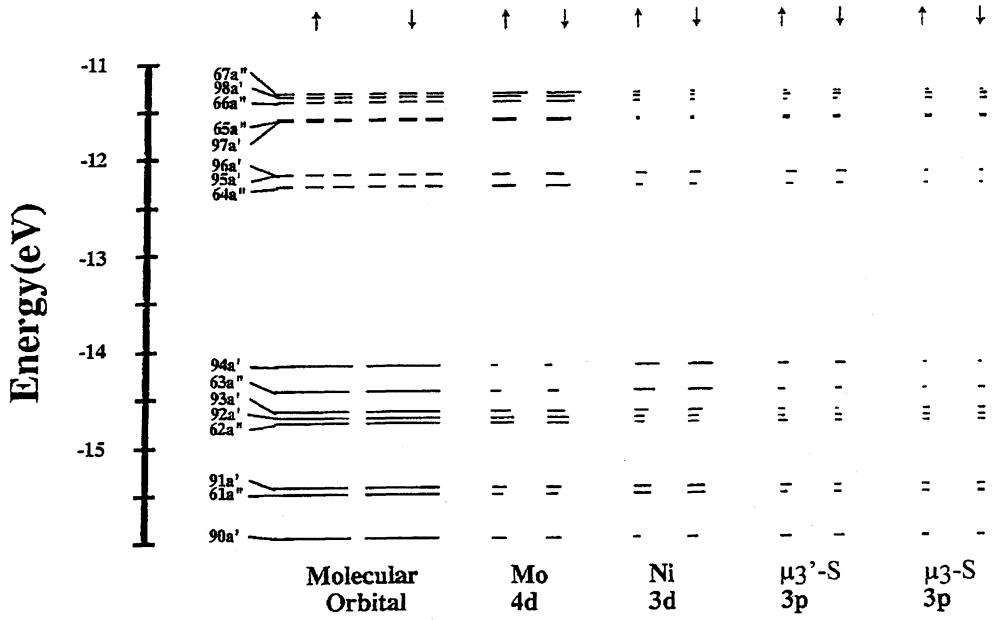

Fig. 7. Energy levels for $[Mo_3NiS_4(H_2O)_{10}]^{4+}$ (**D**). μ_3-S, sulfur atom bridging three molybdenum atoms; μ_3'-S, sulfur atom bridging two molybdenum and one iron atoms.

Calculated transition energies are in fairly good agreement with the experimental ones for both clusters **B** and **D**, as shown in Fig. 14. The transitions at ca. 1.2 eV in **B** are of charge transfer character (from molybdenum to iron), and those at ca. 1.5 eV in **D** also are of charge transfer character, however, the direction is from nickel to molybdenum (see Figs. 6 and 7).

The calculated electronic structures near HOMO and LUMO seems fairly correct as judged by the experimental results such as electronic spectra of **B** and **D**. However, the structures of the one-electron reduced species of **B** and **D** appear rather different from those of **B** and **D** before reduction, and we should not discuss the electronic structures of the reduced species using the energy levels depicted in Figs. 6 and 7.

XPS Spectra. The valence band X-ray photoelectron spectrum of **B′** is shown in Fig. 15 together with calculated values, which correspond well to the experimental peak positions of the spectrum as a whole: shoulders at around 18 and 28 eV in the experimental

Table 6. Orbital Population and Net Charge in $[Mo_3FeS_4(H_2O)_{10}]^{4+}$ (**B**)
Weighted mean values are noted for atoms that are different from each other under C_s symmetry.

	Mo		Fe		μ_3'-S[a]		μ_3-S[b]		O(Fe)		O(trans)[c]		O(cis)[d]		H(Fe)		H(trans)[e]		H(cis)[f]	
	↑	↓	↑	↓	↑	↓	↑	↓	↑	↓	↑	↓	↑	↓	↑	↓	↑	↓	↑	↓
1s	1.000	1.000	1.000	1.000	1.000	1.000	1.000	1.000	1.000	1.000	1.000	1.000	1.000	1.000	0.385	0.385	0.400	0.400	0.406	0.405
2s	1.000	1.000	1.000	1.000	1.000	1.000	1.000	1.000	0.795	0.796	0.799	0.799	0.800	0.798						
2p	3.000	3.000	3.000	3.000	3.000	3.000	3.000	3.000	2.233	2.185	2.220	2.219	2.211	2.213						
3s	1.000	1.000	1.000	1.000	0.899	0.899	0.890	0.890												
3p	3.000	3.000	2.999	2.998	1.901	1.905	1.936	1.922												
3d	5.000	5.000	4.375	2.047	0.149	0.153	0.175	0.174												
4s	0.998	0.998	0.296	0.278																
4p	2.992	2.992	0.609	0.482																
4d	2.143	2.313																		
5s	0.242	0.244																		
5p	0.517	0.521																		
Net charge	0.107	−0.068	−1.278	1.194	0.051	0.043	−0.001	0.014	−0.028	0.019	−0.020	−0.018	−0.011	−0.011	0.115	0.115	0.100	0.100	0.094	0.095
(Net) ↑+↓	0.039		−0.084		0.094		0.014		−0.009		−0.037		−0.022		0.230		0.199		0.189	

a) μ_3'-S: Sulfur atom bridging two molybdenum and one iron atoms. b) μ_3-S: Sulfur atom bridging three molybdenum atoms. c) O(trans): Oxygen atom trans to μ_3-S. d) O(cis): Oxygen atom cis to μ_3-S. e) H(trans): Hydrogen atom bonded to O(trans). f) H(cis): Hydrogen atom bonded to O(cis).

Table 7. Orbital Population and Net Charge in $[Mo_3NiS_4(H_2O)_{10}]^{4+}$ (**D**)
Weighted mean values are noted for atoms that are different from each other under C_s symmetry.

	Mo		Ni		μ_3'-S[a]		μ_3-S[b]		O(Ni)		O(trans)[c]		O(cis)[d]		H(Ni)		H(trans)[e]		H(cis)[f]	
	↑	↓	↑	↓	↑	↓	↑	↓	↑	↓	↑	↓	↑	↓	↑	↓	↑	↓	↑	↓
1s	1.000	1.000	1.001	1.001	1.000	1.000	1.001	1.001	1.001	1.001	1.000	1.000	1.000	1.000	0.391	0.391	0.400	0.400	0.407	0.407
2s	1.000	1.000	1.001	1.001	1.000	1.000	1.001	1.001	0.791	0.791	0.797	0.797	0.799	0.799						
2p	3.000	3.000	3.001	3.001	3.000	3.000	3.001	3.001	2.221	2.221	2.218	2.218	2.212	2.212						
3s	1.000	1.000	1.001	1.001	0.898	0.898	0.891	0.891												
3p	3.000	3.000	3.001	3.001	1.886	1.886	1.921	1.921												
3d	5.000	5.000	4.251	4.251	0.154	0.154	0.171	0.171												
4s	0.998	0.998	0.291	0.291																
4p	2.993	2.993	0.571	0.571																
4d	2.219	2.219																		
5s	0.243	0.243																		
5p	0.517	0.517																		
Net charge	0.030	0.030	−0.111	−0.111	0.061	0.061	0.017	0.017	−0.018	−0.018	−0.015	−0.015	−0.011	−0.011	0.114	0.114	0.100	0.100	0.093	0.093
(Net) ↑+↓	0.061		−0.221		0.123		−0.034		−0.035		−0.030		−0.022		0.228		0.200		0.187	

a) μ_3'-S: Sulfur atom bridging two molybdenum and one nickel atoms. b) μ_3-S: Sulfur atom bridging three molybdenum atoms. c) O(trans): Oxygen atom trans to μ_3-S. d) O(cis): Oxygen atom cis to μ_3-S. e) H(trans): Hydrogen atom bonded to O(trans). f) H(cis): Hydrogen atom bonded to O(cis).

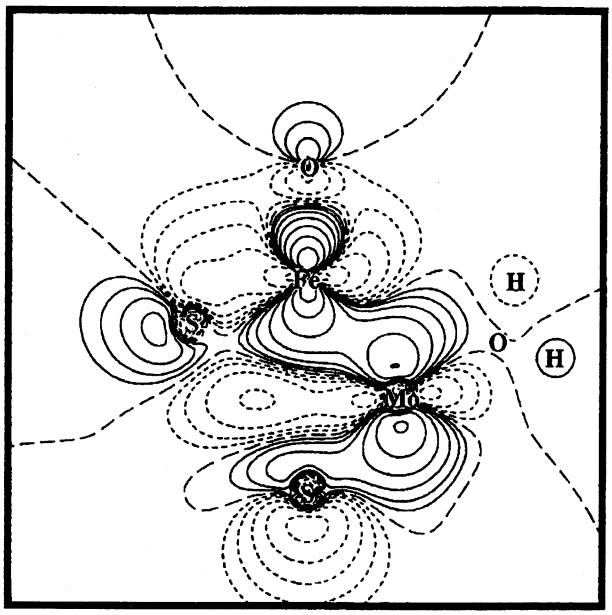

Fig. 8. Contour map (x–z plane) of HOMO (93a'$_\downarrow$) for $[Mo_3FeS_4(H_2O)_{10}]^{4+}$ (**B**). Solid, dotted, and dashed lines indicate positive, negative, and zero contour lines, respectively.

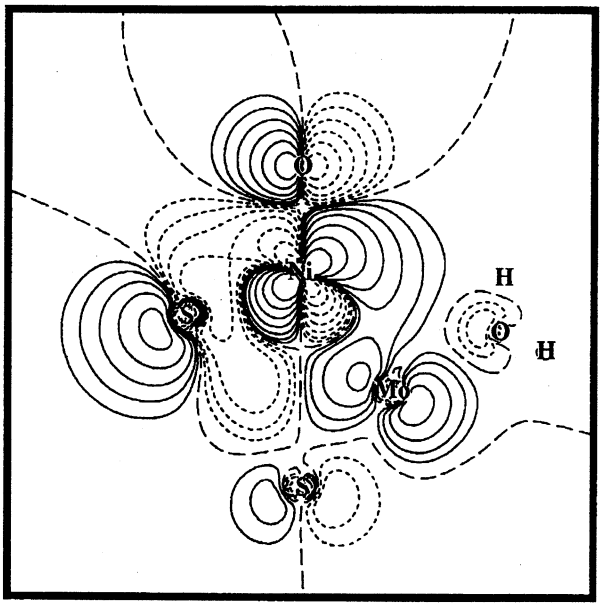

Fig. 9. Contour map (x–z plane) of HOMO (94a') for $[Mo_3NiS_4(H_2O)_{10}]^{4+}$ (**D**). Solid, dotted, and dashed lines indicate positive, negative, and zero contour lines, respectively.

spectrum are attributable to pts^- anion.

We obtained binding energies of Mo $3d_{3/2}$ and Mo $3d_{5/2}$ from the XPS spectra of **A'**, **B'**, **C'**, and **D'**, which are compared with those of calculated orbital energy values as given in Table 8. The order of the calculated orbital energy values ($E_A > E_D > E_B > E_C$) agrees well with the order of the binding energies from XPS. In conformity with the view "the reductive addition of iron or nickel metal to **A**", the orders $E_A > E_B$ and $E_A > E_D$ are observed from the XPS measurement. The magnitude of the binding energy difference between **B** and **C** is similar to that between **A** and **B**, which may apper to indicate that real charge transfer from the incorporated iron atom to **A** is not large. However, the data that the binding energy in **C** is lower than that in **B** can be explained by the fact that the electronegativity of nitrogen in **C** is lower than that of oxygen in **B**, which will make the molybdenum atoms in **C** more electron-rich than those in **B**.

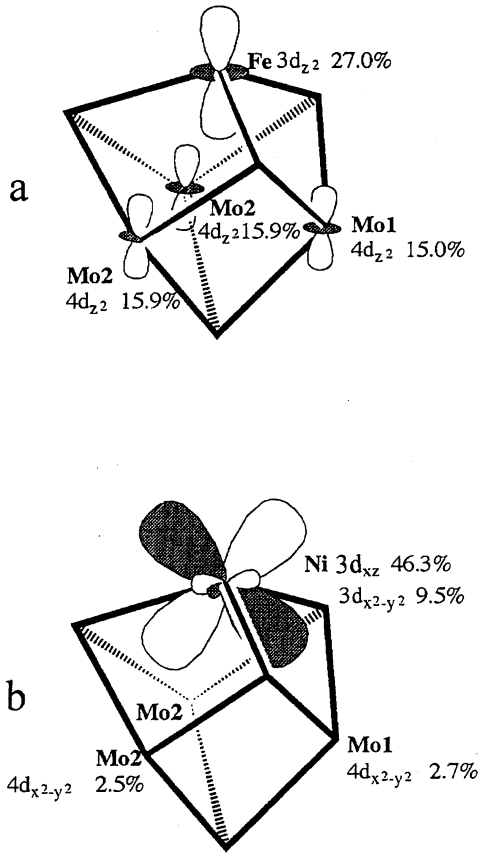

Fig. 10. Atomic orbital components constituting HOMO's: a, $[Mo_3FeS_4(H_2O)_{10}]^{4+}$ (**B**) (93a' $\downarrow$); b, $[Mo_3NiS_4(H_2O)_{10}]^{4+}$ (**D**) (94a').

Table 8. Binding Energies Obtained from XPS, and Calculated Orbital Energy Levels (eV) for $[Mo_3S_4(H_2O)_9](pts)_4 \cdot 9H_2O$ (**A'**), $[Mo_3FeS_4(H_2O)_{10}](pts)_4 \cdot 7H_2O$ (**B'**), $[Mo_3FeS_4(H_2O)(NH_3)_9]Cl_4$ (**C'**), and $[Mo_3NiS_4(H_2O)_{10}](pts)_4 \cdot 7H_2O$ (**D'**)[a)]

	Exptl		Calcd
	Mo $3d_{3/2}$	Mo $3d_{5/2}$	Mo 3d
A'	233.7	230.7	234.1
B'	233.1	230.0	233.3
C'	232.6	229.4	232.8
D'	233.3	230.3	233.6

a) C_{1s}=285.0 eV.

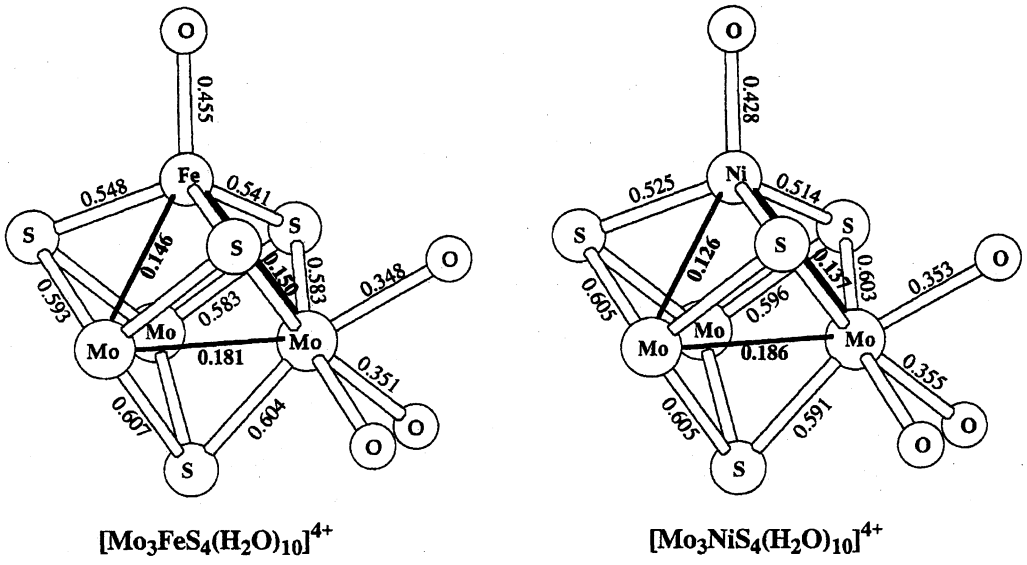

Fig. 11. Bond orders for $[Mo_3FeS_4(H_2O)_{10}]^{4+}$ (**B**) and $[Mo_3NiS_4(H_2O)_{10}]^{4+}$ (**D**).

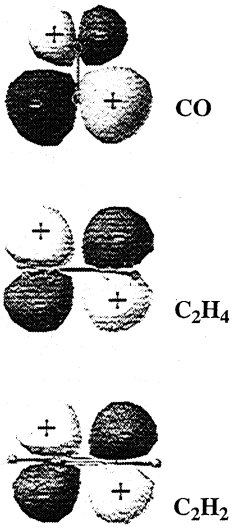

Fig. 12. LUMO's for CO, C_2H_2, and C_2H_4.

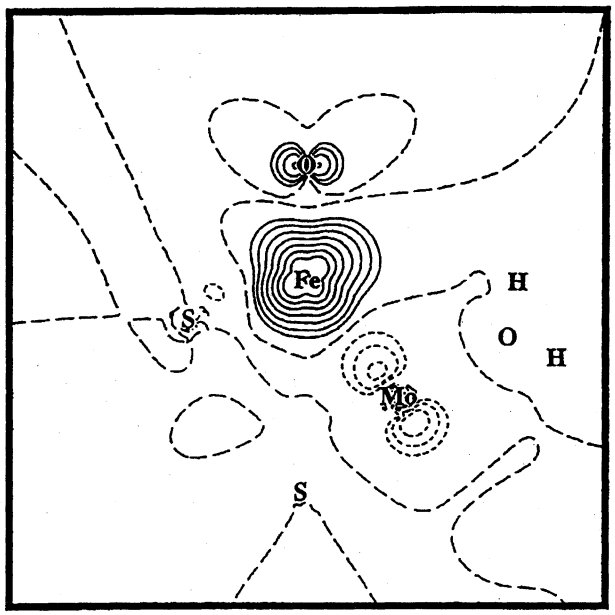

Fig. 13. Effective spin density ($\Delta\rho=\rho_\uparrow-\rho_\downarrow$) of the paramagnetic species $[Mo_3FeS_4(H_2O)_{10}]^{4+}$ (**B**).

In conclusion the formal oxidation states of metals in **B**, **C**, and **D** are more adequately expressed as $Mo^{IV}Mo^{III}{}_2M^{II}$ (M=Fe, Ni) than $Mo^{IV}{}_3M^0$, if we take the experimental results of Mössbauer spectroscopy, electrochemistry, and XPS into consideration.

Supplementary Material Available: The crystallographic and machine data for **B′** and **C′** are given in Tables S1 and S2 for **B′** and **C′**, respectively. Anisotropic thermal parameters for **B′** and **C′** are listed in Tables S3 and S4, respectively. Bond distances and angles are collected in Tables S5 and S6 for **B′** and **C′**, respectively. Short contacts are listed in Tables S7 and S8 for **B′** and **C′**, respectively. Tables S9, S10, and S11 present the ground state energies (eV) and the Mulliken populations (%) of each level for the constituent atoms for **B**, **C**, and **D**, respectively. The F_o-F_c tables for **B′** and **C′** are deposited as Document No. 68042 at the Office of the Editor of Bull. Chem. Soc. Jpn.

We are grateful to Professor H. Kuroya for helpful discussions, and to Professors M. Katada and H. Sano of Tokyo Metropolitan University for the measurement of Mössbauer spectra. We wish to thank Mr. H. Takagi for the electrochemical measurements. This work was partly supported by a Grant-in-Aid for Scientific Research Nos. 59470039, 02453043, and 04241102 (on Pri-

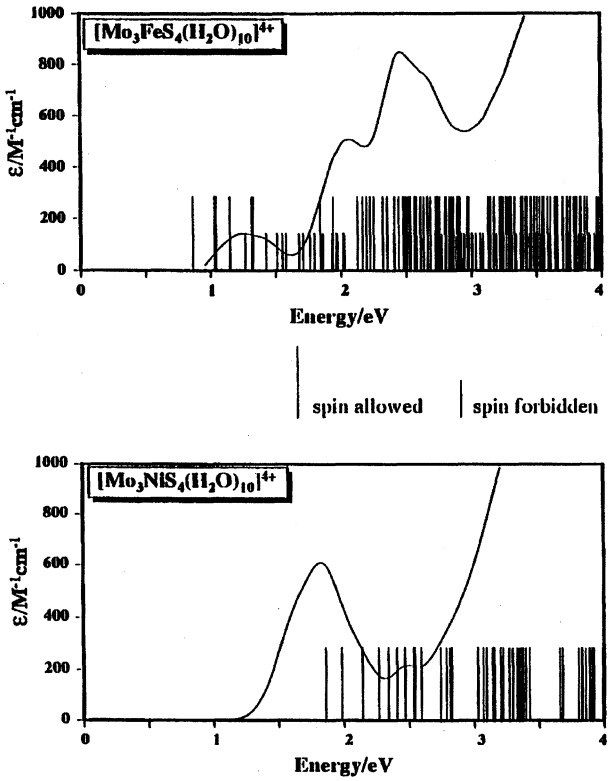

Fig. 14. Electronic spectra: a, $[Mo_3FeS_4(H_2O)_{10}]^{4+}$ (**B**); b, $[Mo_3NiS_4(H_2O)_{10}]^{4+}$ (**D**). The long and short lines indicate spin allowed and spin forbidden transition, respectively.

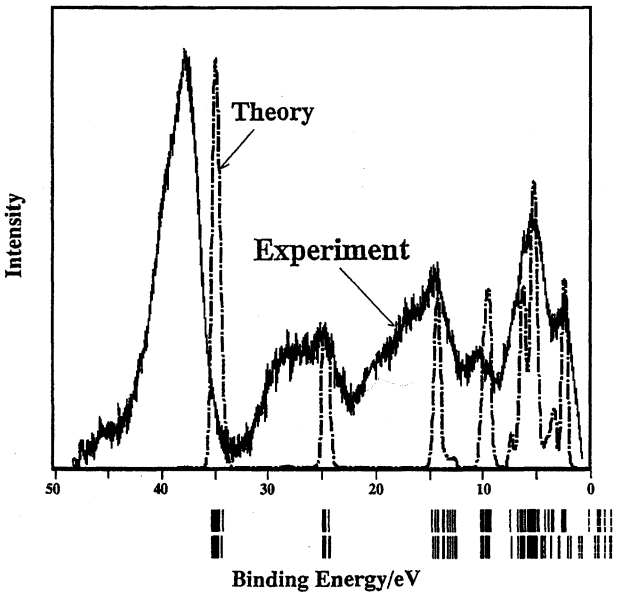

Fig. 15. Valence band X-ray photoelectron spectrum of $[Mo_3FeS_4(H_2O)_{10}](CH_3C_6H_4SO_3)_4 \cdot 7H_2O$ (**B′**). (a) Experiment, measured after dehydration, (b) Theory, calculated with 0.5 eV as half-width for a single level, excluding contributions from the anion pts^- and water of crystallization (shifted linearly by 12.2 eV to lower energies to fit the calculated trace to the experimental one). Under the abscissa calculated values without half-width are shown.

ority Area of "Activation of Inactive Small Molecules") from the Ministry of Education, Science and Culture.

References

1) T. Shibahara, H. Akashi, and H. Kuroya, *J. Am. Chem. Soc.*, **108**, 1342 (1986).

2) a) M=Ni: T. Shibahara and H. Kuroya, *J. Coord. Chem.*, **18**, 233 (1988); b) M=Ni: T. Shibahara, M. Yamasaki, H. Akashi, and T. Katayama, *Inorg. Chem.*, **30**, 2693 (1991); c) M=Cu: T. Shibahara, H. Akashi, and H. Kuroya, *J. Am. Chem. Soc.*, **110**, 3313 (1988); d) M=Sn: H. Akashi and T. Shibahara, *Inorg. Chem.*, **28**, 2906 (1989); e) M=Co, Hg: T. Shibahara, H. Akashi, M. Yamasaki, and K. Hashimoto, *Chem. Lett.*, **1991**, 689; f) M=In: G. Sakane and T. Shibahara, *Inorg. Chem.*, **32**, 777 (1993); g) M=Sb: T. Shibahara, K. Hashimoto, and G. Sakane, "Abstract of the Fifth International Conference on Bioinorganic Chemistry, Oxford," *J. Inorg. Biochem.*, **43**, 280 (1991).

3) a) M=Pd: T. Murata, H. Gao, Y. Mizobe, F. Nakano, S. Motomura, T. Tanase, S. Yano, and M. Hidai, *J. Am. Chem. Soc.*, **114**, 8287 (1992); b) M=Fe: P. W. Dimmock, D. P. E. Dickson, and A. G. Sykes, *Inorg. Chem.*, **29**, 5120 (1990); c) M=Ni, Fe: P. W. Dimmock, G. J. Lamprecht, and A. G. Sykes, *J. Chem. Soc., Dalton Trans.*, **1991**, 955; d) M=Cr: C. A. Routledge, M. Humanes, Y.-J. Li, and A. G. Sykes, *J. Chem. Soc., Dalton Trans.*, **1994**, 1275.

4) a) X.-T. Wu, S.-F. Lu, L.-Y. Zu, Q.-I. Wu, and J.-X. Lu, *Inorg. Chim. Acta*, **133**, 39 (1987); b) S.-F. Lu, J.-Q. Huang, Y.-H. Lin, and J.-L. Huang, *Huaxue Xuebao*, **45**, 666 (1987); c) J.-Q. Huang, J.-L. Huang, M.-Y, Shang, S.-F. Lu, X.-T. Lin, Y.-H. Lin, M.-D. Huang, H.-H. Zhuang, and J.-X. Lu, *Pure Appl. Chem.*, **60**, 1185 (1988).

5) A. Deeg, H. Keck, A. Kruse, W. Kuchen, and H. Wunderlich, *Z. Naturforsch., B*, **43B**, 1541 (1988).

6) T. Shibahara, G. Sakane, and S. Mochida, *J. Am. Chem. Soc.*, **115**, 10408 (1993).

7) T. Shibahara and G. Sakane, unpublished result.

8) T. Shibahara, T. Asano, and G. Sakane, *Polyhedron*, **10**, 2351 (1991).

9) M. Nasreldin, Y.-J. Li, F. E. Mabbs, and A. G. Sykes, *Inorg. Chem.*, **33**. 4283 (1994).

10) a) H. Aikoh and T. Shibahara, *Physiol. Chem. Phys. Med. NMR*, **22**, 187 (1990); b) H. Aikoh and T. Shibahara, *Analyst*, **118**, 1329 (1993).

11) T. Murata, Y. Mizobe, H. Gao, Y. Ishii, T. Wakabayashi, F. Nakano, T. Tanase, S. Yano, M. Hidai, I. Echizen, H. Nanikawa, and S. Motomura, *J. Am. Chem. Soc.*, **116**, 3389 (1994).

12) T. Shibahara, S. Mochida, and G. Sakane, *Chem. Lett.*, **1993**, 89.

13) a) T. Shibahara, M. Yamasaki, G. Sakane, K. Minami, T. Yabuki, and A. Ichimura, *Inorg. Chem.*, **31**, 640 (1992); b) T. Shibahara and H. Akashi, *Inorg. Synth.*, **29**, 260 (1992).

14) The yield is based on the ε value of $[Mo_3FeS_4(H_2O)_{10}](CH_3C_6H_4SO_3)_4 \cdot 7H_2O$ (**B′**) dissolved in 1 M HCl.

15) G. M. Shelrick, Institute fuer Anorganische Chemie der Universität, Tammanstrasse 4, D-3400 Goettingen, Germany.

16) "The Universal Crystallographic Computation Program System," The Crystallographic Society of Japan,

Tokyo (1969).
17) C. Katayama, *Acta Crystallogr., Sect. A*, **A42**, 19 (1986).
18) C. K. Johnson, "Report ORNL-3794," Ork Ridge National Laboratory, Oak ridge, TN (1965).
19) "International Tables for X-Ray Crystallography," Kynoch Press, Birmingham, England (1974), Vol. IV.
20) H. Adachi, M. Tsukada, and C. Satoko, *J. Phys. Soc. Jpn.*, **45**, 875 (1978).
21) J. C. Slater, "Symmetry and Energy Bands in Crystals," Dover Publications, Inc., New York, N. Y. (1972), p. 55.
22) M. Katada, H. Akashi, T. Shibahara, and H. Sano, *J. Radioanal. Nucl. Chem., Lett.*, **145**, 143 (1990).
23) T. Shibahara, M. Yamasaki, T. Watase, and A. Ichimura, *Inorg. Chem.*, **33**, 292 (1994).
24) T. Shibahara and H. Kuroya, *Polyhedron*, **5**, 357 (1986).
25) H. Akashi, T. Shibahara, and H. Kuroya, *Polyhedron*, **9**, 1671 (1990).
26) The μ_3'-S's correspond to μ_2-S's in **A**$'$.
27) H. Akashi, N. Uryu, and T. Shibahara, details to be published.
28) H. Kobayashi, T. Shibahara, and N. Uryu, *Bull. Chem. Soc. Jpn.*, **63**, 799 (1990).
29) See, for example: a) H. Adachi and M. Takano, *J. Solid State Chem.*, **93**, 556 (1991); b) H. Adachi, S. Shiokawa, M. Tsukada, C. Satoko, and S. Sugano, *J. Phys. Soc. Jpn.*, **47**, 1528 (1979).
30) T. Shibahara and G. Sakane, to be published.
31) Calculation using the EHMO method.